

Geophysical Research Letters[®]



RESEARCH LETTER

10.1029/2022GL098771

Intermittent Behavior in the AMOC-AMV Relationship

Alessio Bellucci¹ , Denis Mattei², Paolo Ruggieri³ , and Luca Famooss Paolini^{4,5} 

Key Points:

- Spontaneous breakings of the Atlantic meridional overturning circulation-Atlantic multidecadal variability (AMOC-AMV) connection are found in a suite of multi-century control simulations from the 6th phase of the Coupled Model Inter-comparison Project
- The inception and demise of these AMOC-AMV de-coupling events can be abrupt in scale and last several decades or centuries
- Decoupling between AMOC and AMV is more likely to occur when their respective variance is low

Supporting Information:

Supporting Information may be found in the online version of this article.

Correspondence to:

A. Bellucci,
a.bellucci@isac.cnr.it

Citation:

Bellucci, A., Mattei, D., Ruggieri, P., & Famooss Paolini, L. (2022). Intermittent behavior in the AMOC-AMV relationship. *Geophysical Research Letters*, 49, e2022GL098771. <https://doi.org/10.1029/2022GL098771>

Received 18 MAR 2022

Accepted 16 AUG 2022

¹Consiglio Nazionale delle Ricerche, Istituto di Scienze dell'Atmosfera e del Clima (CNR-ISAC), Bologna, Italy, ²University of Modena-Reggio Emilia, Modena, Italy, ³Department of Physics and Astronomy, University of Bologna, Bologna, Italy, ⁴Fondazione Centro Euro-Mediterraneo sui Cambiamenti Climatici (CMCC), Bologna, Italy, ⁵University of Venice Ca' Foscari, Venice, Italy

Abstract The connection between the Atlantic meridional overturning circulation (AMOC) and the Atlantic multidecadal variability (AMV) is inspected in a suite of pre-industrial integrations from the 6th phase of the Coupled Model Inter-comparison Project (CMIP6), using a change-point detection method to identify different AMOC-AMV co-variability regimes. A key finding of this study is that models robustly simulate multi-decadal windows where the AMV and the AMOC are essentially uncorrelated. These regimes coexist with longer periods with relatively high correlation. Drops and recoveries of correlation are found to be often abrupt and confined in a temporal window of the order of 10 years. Phenomenological evidence suggests that the no-correlation regimes may be explained by drops in the variance of the AMOC: a less variable meridional heat transport leads to a suppressed co-variability of the AMV, leaving a larger role for non-AMOC drivers, consistent with a non-stationary AMOC-stationary noise interpretative framework.

Plain Language Summary The North Atlantic Ocean exhibits prominent multi-decadal variability, modulating the climate and weather of the surrounding continental regions. A relevant fraction of this variability is explained by the interplay between ocean circulation and heat transport, leading to coordinated, basin-wide fluctuations in surface temperatures. In this study we analyze the multi-century stability of this interaction in a suite of climate model simulations, providing evidence for the occurrence of spontaneous breakings in the connection between ocean circulation and ocean surface temperatures. These events can be abrupt in time, last from decades to centuries, and are associated with synchronous changes in the characteristics of the oceanic variability. A conceptual model is provided to interpret these transitions. These findings raise concern about the potential occurrence of similar decoupling episodes in the future, and the need for adequately long observational records to fully represent the long-term modulation of multi-decadal variability in the Atlantic sector.

1. Introduction

The origin of the observed multi-decadal swings in the North Atlantic sea-surface temperatures (SSTs), conventionally referred to as Atlantic multidecadal variability (AMV), is at the core of a highly controversial debate (Clement et al., 2015; Mann et al., 2021; Zhang et al., 2019). In the context of the historical climate record (past 150 years), different processes have been suggested as drivers of the observed AMV-related fluctuations, including internal variations of the Atlantic meridional overturning circulation (AMOC; Gulev et al., 2013), natural forcings (Otterå et al., 2010; Swingedouw et al., 2015) and changes in anthropogenic aerosols and green-house gases (Bellucci et al., 2017; Booth et al., 2012). Under fixed external forcing conditions, the AMOC-AMV connection emerges as a key element of the low-frequency variability in the Atlantic region (Ba et al., 2014; Delworth & Mann, 2000; Knight et al., 2005) with changes in the AMOC strength leading, through a delayed response in the poleward heat transport, to a modulation of the SSTs on a basin-wide scale. This causal chain has relevant implications for the climate predictability of the Atlantic region on decadal and longer time scales. Decadal hindcasts performed with global climate models initialized with realistic estimates of the climate state display significant skill in retrospective predictions of SSTs over the North Atlantic subpolar gyre, suggesting a role for the initialization of the ocean through synchronization of predicted and observed AMOC and heat transport fluctuations (Robson et al., 2014; Yeager & Robson, 2017). The stability of the AMOC-AMV connection is therefore instrumental for the predictability of the North Atlantic climate anomalies: a temporary weakening or disruption of this mechanism might negatively affect the predictive ability of decadal forecast systems in the Atlantic sector.

© 2022. The Authors.

This is an open access article under the terms of the [Creative Commons Attribution License](https://creativecommons.org/licenses/by/4.0/), which permits use, distribution and reproduction in any medium, provided the original work is properly cited.

Analyses of the stationarity of some of the dominant variability modes in the climate system have shown that internally generated variability can spontaneously arise in long control simulations of the climate system leading to significant modulations of the process under exam. Wittenberg. (2009) found inter-centennial modulations of the ENSO signal in a 2,000-year control simulation of the pre-industrial climate. Mavilia et al. (2018) analyzed the AMV stationarity in an ensemble of CMIP5 pre-industrial simulations, highlighting the alternation of epochs with significantly different regimes of North Atlantic SST low-frequency variability.

In this study we focus on the stationarity of the AMOC-AMV relationship over multi-century and longer scales. Due to the brevity of the observational records and the poor reliability of paleoclimate proxy records in the multi-decadal range (Caesar et al., 2021), we here examine a multi-model ensemble including the longest available pre-industrial simulations from the 6th phase of the Coupled Model Inter-comparison Project (CMIP6) archive. A methodology is devised to robustly identify changes in the AMOC-AMV co-variability. This methodology is then applied to all long (>700-year) pre-industrial simulations in CMIP6, highlighting the systematic occurrence of abrupt transitions between correlated and non-correlated AMOC-AMV regimes. This peculiar class of events and their relation with specific features of the AMOC and AMV variability are discussed, and a conceptual model schematizing their phenomenology is described.

2. Materials and Methods

2.1. Low Frequency Variability Indices: AMV and AMOC

The AMV index is diagnosed from annual mean SST anomalies, area averaged over the [0°N–60°N; 75°W–7.5°W] latitude-longitude domain in the North Atlantic. A 10-year low-pass filter is then applied to the resulting time series. The AMOC index is obtained from annual mean meridional overturning streamfunction anomalies, spatially averaged over the [25°N–50°N, 500–1,500 m] latitude-depth range in the North Atlantic sector. For consistency with the AMV index, a 10-year low-pass filter is also applied to the AMOC index.

2.2. Change-Point Detection Method

The AMV and AMOC co-variability is characterized through a multi-step procedure, outlined below. First, for each model an 80-year moving window correlation of AMV and AMOC time series is calculated. The resulting running correlation function $c(t)$ is then segmented into different *regimes*, that is, periods during which the correlation values oscillate around a certain reference value. To determine this segmentation in a reproducible way, a change-point detection method is applied. In general, change-points are those points in a data sequence where a change in the statistical properties (such as mean, median, variance, etc.) is found (Haynes et al., 2014). Formally speaking, we assume $c(t)$ to be a multivariate piecewise stationary random process $y_{1:n} = (y_1 \dots y_n)$, where n is the length of the time series. It is assumed that some characteristics of the signal change at some unknown instants $\tau_1 < \tau_2 \dots < \tau_m$, where m is the number of change-points, $\tau_0 = 0$ and $\tau_{m+1} = n$. Change point detection consists in estimating the indices τ_i with $1 \leq i \leq m$. Formally, the change point detection is a parametric-model selection problem that consists in choosing the best segmentation based on a quantitative criterion which must be minimized. This criterion is commonly formalized as a minimization of the following expression:

$$\sum_{i=1}^{m+1} \left[C \left(y_{(\tau_{i-1}+1):\tau_i} \right) \right] + \beta f(m) \quad (1)$$

where C is a cost function and $\beta f(m)$ is a penalty term introduced to prevent over-fitting. The cost function is used to evaluate the goodness-of-fit of the data ranging from τ_{i-1} to τ_i to a specific parametric model. The choice of the cost function depends on the statistical property changings we want to detect (e.g., mean, median, variance, or other statistical properties). Penalty measures the complexity of the model and increases with the number of change-points according to m . To control the trade-off between complexity and goodness-of-fit (measured by the sum of costs) one uses the parameter β , so that a segmentation in many regimes is favored by a low value of β , while high values of β reject most change points. Different search point methods exist that allow to solve the problem of minimizing the Equation 1, yielding either exact or approximate solutions.

For this study, a cost function detecting shifts in the median of the AMOC-AMV moving correlation is selected, while for the search point method the Pruned Exact Linear Time scheme is used (Killick et al., 2012). The latter is

an exact method whose computational cost scales linearly with the number of data points. Regarding the choice of the penalty term, following the Akaike Information Criterion (Akaike, 1974), we set $\beta = 2p$ where p is the number of parameters added when the algorithm finds a new change point. Since every time we find a new change point we add one change point and one median, the number of parameters is $p = 2$, and $\beta = 4$. Finally, we set $f(m) = m$, meaning that we assume a model complexity linearly increasing with the number of the change points.

The change-point detection procedure allows the identification of different AMOC-AMV correlation regimes, that is, temporal segments characterized by $c(t)$ fluctuations around a certain median value. The partition of the full $c(t)$ series into piecewise stationary segments highlights the occurrence of time intervals characterized by a different degree of AMOC-AMV coupling. As a next step, the statistical significance of the AMOC-AMV correlation is assessed according to a one-tailed t-Student statistical test assuming as a null hypothesis that the variables are not correlated, with a 99% significance level. The autocorrelation in the time series, which reduces the effectively independent data, is accounted for through the computation of the effective sample size, following Bretherton et al. (1999). Once the change-point detection is completed, a statistical significance test is applied for each time segment. If, for a given segment, the number of significant correlation occurrences exceeds the 60% of the total, that segment is identified as a “correlation regime” (hereafter, CR). On the other hand, time segments presenting more than 60% of values below the statistical significance level are labeled as “non-correlated regime” (hereafter, NCR). This procedure is then routinely applied to every model $c(t)$ time series, providing a quantitative and statistically grounded criterion to characterize the AMOC-AMV co-variability in terms of CR and NCR regimes.

2.3. Estimation of Probability Density Functions

PDFs are computed with a kernel density estimation with Gaussian kernels. The bandwidth is selected following Scott (1992). PDFs for CR and NCR events (red and blue curves in Figures 4a and 4b) are normalized by the total number of events.

3. Pre-Industrial Climate Simulations and Models

A multi-model ensemble of control simulations from the CMIP6 (Eyring et al., 2016) is evaluated. Specifically, ten multi-century integrations of the pre-industrial climate, forced with time-invariant radiative forcing conditions (including greenhouse gases, ozone, aerosol loadings, and solar irradiance) representative of year 1850 are inspected. The absence of non-stationarities associated with an external forcing provides an optimal experimental setup to investigate internally generated climate fluctuations. The models used in the analysis and their relative simulation lengths are reported in Table S1 in Supporting Information S1. In order to allow an adequate sampling of the multidecadal scale in the AMV and AMOC signals, only model integrations with a minimum 700-year length were selected.

4. Results

The global ocean-atmosphere models used for this analysis (listed in Table S1 in Supporting Information S1) feature significant multi-decadal variability in the North Atlantic sector, with ~ 0.1 K SST fluctuations (reproducing the observed AMV-like horse-shoe pattern; not shown), and ~ 1 Sv ($1 \text{ Sv} = 10^6 \text{ m}^3 \text{ s}^{-1}$) AMOC anomalies (Figure S1 in Supporting Information S1). Two models (EC-Earth3_r2 and IPSL-CM6-LR) exhibit a prominent quasi-regular oscillation with a dominant ~ 200 -year periodicity (see Jiang et al. (2021) for a detailed description of this AMOC oscillation in the IPSL-CM6-LR model). Also, in all models, the AMOC leads the AMV, with a lag of 1–2 years (except for INM-CM5 and MRI-ESM2 featuring longer 3-year and 5-year lags, respectively; not shown) consistent with previous assessments of CMIP pre-industrial climate simulations (e.g., Tandon & Kushner, 2015).

Figure 1 shows the time series of the 80-year sliding-window AMOC-AMV correlation $c(t)$ for each individual model, with indications of the different AMOC-AMV co-variability regimes, identified following the methodology outlined in Section 2. The $c(t)$ series are punctuated by sharp, decadal scale fluctuations between significantly correlated and non-correlated regimes (hereafter CR and NCR, respectively). The NCR regimes can have a duration ranging from a few decades up to several centuries, and their inception and termination are

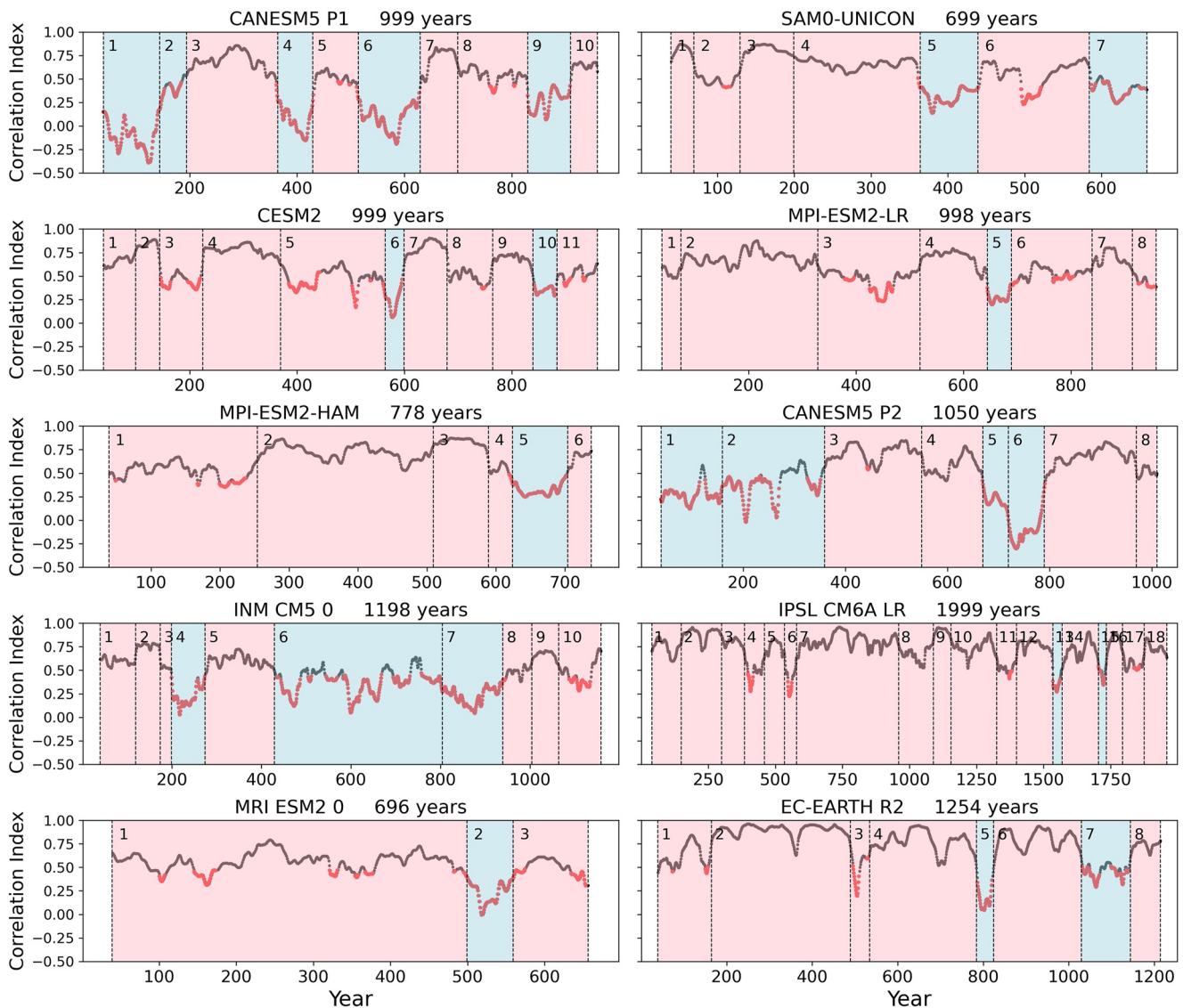


Figure 1. Moving Atlantic meridional overturning circulation-Atlantic multidecadal variability (AMOC-AMV) correlation coefficient, computed using an 80-year sliding window. Prior to the correlation calculation, AMV and AMOC time series are shifted by the time-lag that maximizes their correlation. The *correlated regimes* are highlighted in pink, while *non-correlated regimes* are highlighted in light blue. Vertical dashed lines mark the change-points in moving correlations (see Materials and methods). The red points indicate the correlation values that are not statistically significant.

generally marked by symmetrically rapid transitions. These occurrences are detected in every scrutinized model, and appear to be irregularly scattered in time (within an individual simulation) and across models. The relative fraction of CR- versus NCR-years is a strongly model-dependent feature, with some models showing an almost equal partition between the two regimes (notably, CanESM5-p1 and -p2 and INM-CM5-0), contrasting with models where the CR regime largely prevails (e.g., IPSL-CM6-LR). It is also worth noting that, during the CR regimes, $c(t)$ values in excess of 0.7 are often found, confirming that a strongly coupled AMOC-AMV regime is a plausible state in the context of unforced simulations of the pre-industrial climate. At the same time, the potential occurrence of spontaneous breakings (i.e., not forced by changes of control parameters) of this linkage in an ensemble of state-of-the-art climate models raises the issue of the inadequacy of the available observational record to properly constrain the full spectrum of natural variability in the North Atlantic area.

The robustness of these results to changes in the length of the sliding window has been tested, using 60- and 100-year widths, in alternative to the selected 80-year value. Aim of the test was to verify whether both the occurrence and timing of the change-points were sensibly affected by the window length parameter. According to this

analysis, the relative fraction of CR versus NCR years is expectedly sensitive to the window length parameter, with a tendency for NCR/CR years ratio to decrease for increasing window lengths. However, the emerging picture of spontaneous AMOC-AMV decoupling episodes, leading to decadal and multidecadal NCR regimes remains qualitatively unchanged.

Next, we characterize the nonstationary behavior featured by the AMOC-AMV connection in terms of the spectral features of AMV and AMOC signals.

In Figure 2, the wavelet power spectra (Torrence & Compo, 1998) of AMV and AMOC time series are shown for the examined models, together with the indications of the corresponding CR and NCR regimes. At a first glance, all models display multi-centennial modulations of the spectral power over specific frequency bands. The non-stationarity associated with the low frequency behavior of AMOC and AMV is particularly prominent in the multi-decadal (30–100 years) range, with spectral peaks exceeding the climate noise level for several decades/centuries, before fading under the level of significance. The connection between these spectral non-stationarities and the regime transitions identified in the AMOC-AMV moving correlation is examined. Some of the simulations provide particularly insightful examples of this linkage. For instance, MRI-ESM2-0 and MPI-ESM2-HAM share a very similar AMOC-AMV co-variability, with a single, shorter than 100-year, NCR event, occurring in concomitance with a significant reduction in the AMOC spectral power over the multidecadal range, occurring around model years 500 and 600, respectively. Interestingly, both models show an enhancement in the multidecadal AMV spectral power during the NCR regime, suggesting that the AMOC-AMV decoupling is associated with a change in the AMOC variability only. CanESM5-p1 provides a specular example, with two well distinguishable patches of enhanced AMV power (not mirrored by the AMOC signal) in the CR regimes 3 (100-year period) and 8 (30-year period), both rapidly decaying short before the transition to NCR regimes 4 and 9, respectively. A third illustrative example is given by the INM-CM5-0 model, featuring a decay in the spectral power of AMV and AMOC, primarily over the 100-year period, occurring in correspondence of the 3–4 CR-NCR regime transition, around model year 200. Note that in this case the AMOC leads the AMV power decrease, suggesting that the AMOC-AMV decorrelation is associated with a drop in the AMOC multidecadal variability.

Next, the connection between the transitions detected in the AMOC-AMV moving correlations and the spectral non-stationarities identified through the wavelet analysis is assessed in a more quantitative way. For this purpose, a simple index is defined based on the integral of the AMOC and AMV wavelet amplitudes, computed over the 30–100 years frequency range:

$$L(t) = \int_{S_0}^{S_1} w(s, t) ds \quad (2)$$

where w is the wavelet amplitude (of either AMV or AMOC), s is the frequency, t is the time, and S_0 and S_1 are the integral bounds in the frequency domain, here set equal to 30 and 100 years, respectively. This index is then used to characterize the overall low-frequency, multidecadal scale variability of the AMOC and AMV signals, in proximity of the regime transitions. This is done by computing a composite of the $L(t)$ index for all the CR-NCR and NCR-CR transitions, over a time window of ± 50 -year width centered over each regime change-point, across all events and all models. The composite analysis (Figure 3, left panel) reveals a consistent reduction (increase) in the multidecadal spectral power, as quantified by the integral $L(t)$ index, associated with a CR-NCR (NCR-CR) transition, for both AMOC and AMV. Hints of an asymmetry between CR-NCR and NCR-CR are also visible, with the latter reaching a plateau in a shorter time compared to the former. On the other hand, this signal is affected by a large inter-model uncertainty, as indicated by the large spread around the multi-model mean (Figure 3, right panel).

The relationship between the AMOC-AMV coupling and the variability in the two constituent signals is further elucidated by looking at the moving standard deviation of AMOC and AMV (hereafter, σ_{AMOC} and σ_{AMV}) using a 80-year sliding window, consistent with the moving correlation analysis. The probability density functions (PDF; see Materials and methods) of σ_{AMOC} and σ_{AMV} are shown in Figures 4a and 4b for all models and all years, and further partitioned into CR and NCR only events. It is found that NCR events are overall less frequent than CR events (as expected from Figure 1) and, most importantly, shifted toward lower amplitude values. Also, the range of values in NCR is considerably narrower than in CR regimes, with the latter exhibiting an extended tail of large σ values exceeding 1 Sv and 0.2 K for σ_{AMOC} and σ_{AMV} respectively.

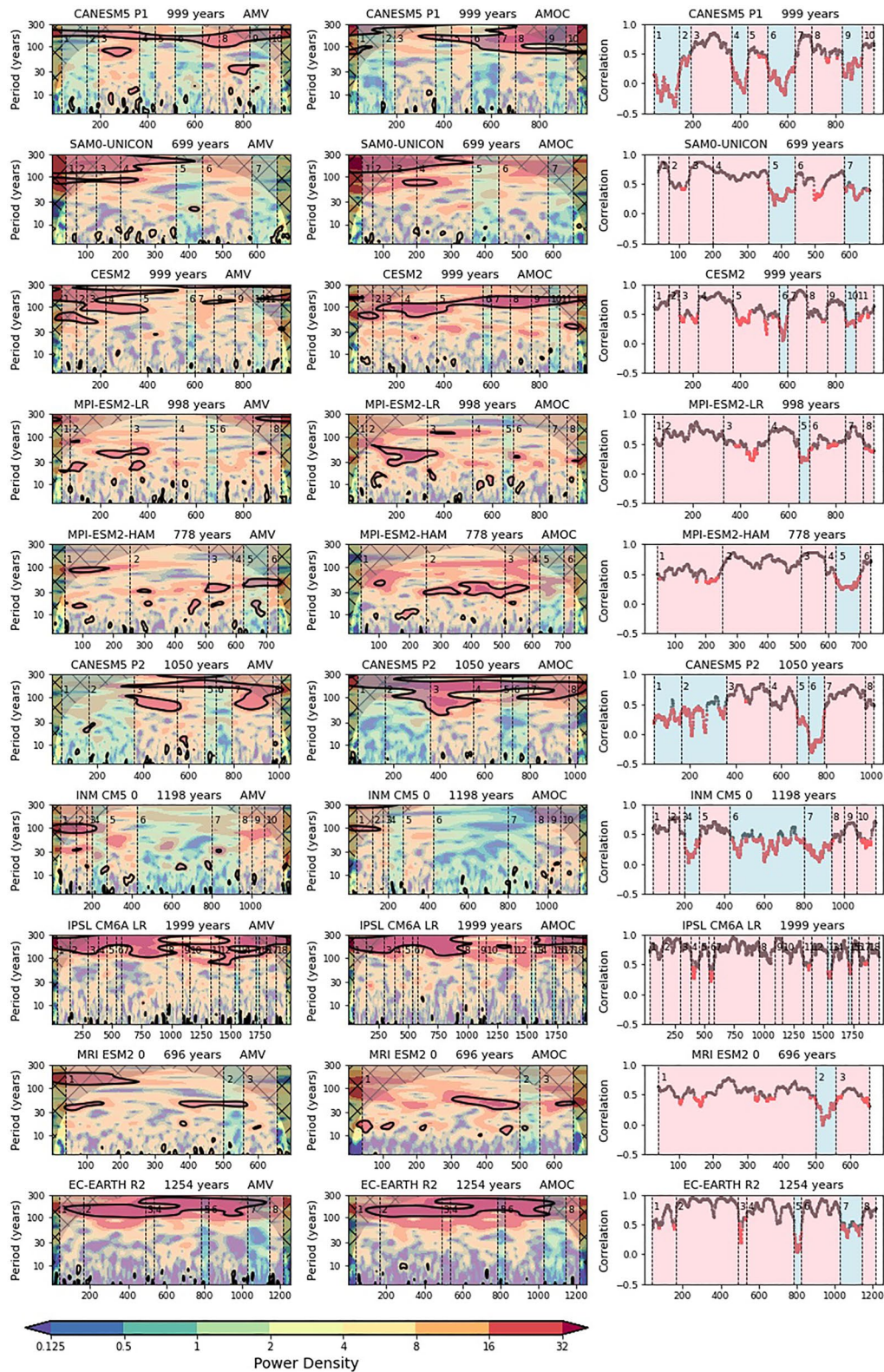


Figure 2. Wavelet power spectra of the Atlantic multidecadal variability (AMV) index and the Atlantic meridional overturning circulation (AMOC) index (left and central columns, respectively). Thick black contours in the wavelet spectra enclose values exceeding the red noise level (95% confidence). Overlapped to the wavelet power, the correlation change-points (vertical dashed lines) and *non-correlated regimes* (light blue shading) are also shown. Moving AMOC-AMV correlations (already shown in Figure 1) are replicated in the right column. Note that unfiltered (i.e., annual mean) values for AMOC and AMV have been used in the wavelet analysis.

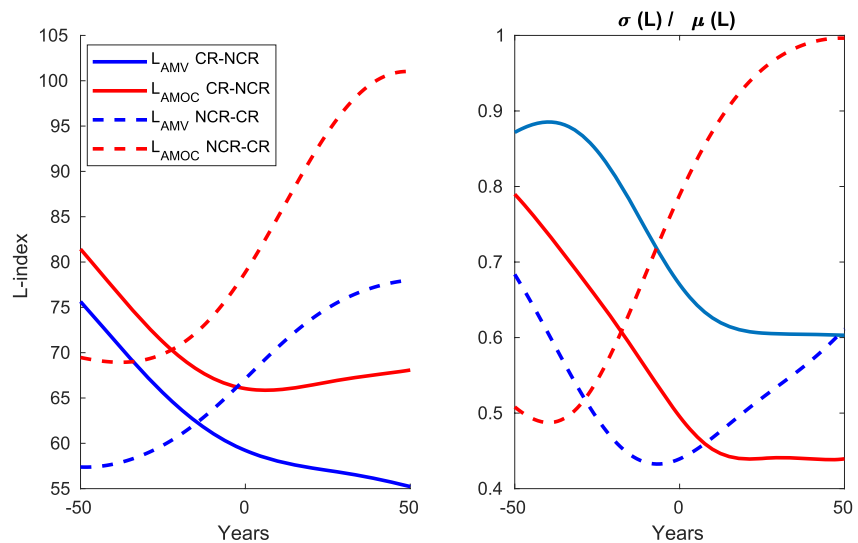


Figure 3. Left: Composite of the $L(t)$ index evaluated across all transition events, over a 100-year wide time window centered on individual change-points, for Atlantic multidecadal variability (blue) and Atlantic meridional overturning circulation (red). Solid (dashed) lines indicate *correlated regimes* (CR) to *non-correlated regimes* (NCR) (NCR to CR) transitions. Right: Uncertainty associated with $L(t)$ index (left panel) evaluated as the ratio between the $L(t)$ multi-event ensemble spread (σ) and the corresponding ensemble mean (μ).

The connection between σ_{AMOC} and σ_{AMV} is illustrated through a scatter plot (Figure 4c). Given the large inter-model differences in the variability amplitude (Figure S1 in Supporting Information S1), σ values are now expressed in standardized units (i.e., for each model, the mean σ value has been removed and the result has been divided by the corresponding standard deviation). The diagonally stretched orientation of the points in the scatter plot highlights that σ_{AMOC} and σ_{AMV} are well correlated in the examined model population (0.54 correlation). The other notable aspect is that the NCR regimes occur primarily in the low variability sub-space (bottom-left corner in the σ_{AMOC} - σ_{AMV} diagram). In other words, the decoupling between the AMOC and AMV signals is more likely to occur when the amplitude of their variability is low. However, this does not rule out the occurrence of low- σ /CR states (red points in the bottom-left corner of the scatter diagram). On the other hand, high- σ /NCR states appear to be far less likely states. Figure 4c is complemented by Figure 4d where the σ centroids for the full multi-model set of CR and NCR regimes, as well as for individual models and regimes, are shown. Note that the multi-model CR centroid in Figure 4d diagram is very close to the origin of the coordinated axes, reflecting the asymmetry between CR and NCR events distributions, with the latter being more likely to occur with low- σ , and the former occurring with either high- or low- σ conditions.

5. Conclusions

In this study we reported on the occurrence of spontaneous, abrupt shifts in the AMOC-AMV co-variability in a multi-model ensemble of pre-industrial CMIP6 simulations. To the authors' knowledge, this is the first study documenting this class of events in state-of-the-art climate models.

A crucial finding of the study is that models robustly simulate multi-decadal windows where the AMV and the AMOC variability are essentially uncorrelated. These regimes coexist with longer periods with relatively high correlation. Drops and recoveries of correlation are found to be often abrupt and confined in a temporal window of the order of 10 years. Metrics adopted in our study do not allow a clean identification of relevant time scales as the use of running windows makes the attribution blurred. Identifying mechanisms for the transition could provide more reliable estimates of their time-scale and clarify the opportunity for their potential prediction. This should be clarified by future efforts.

Alternative hypotheses can be formulated to explain the occurrence of the NCR regimes. Assuming a simplified description of the AMOC-AMV relationship, formulating the AMV as linearly depending on the AMOC signal

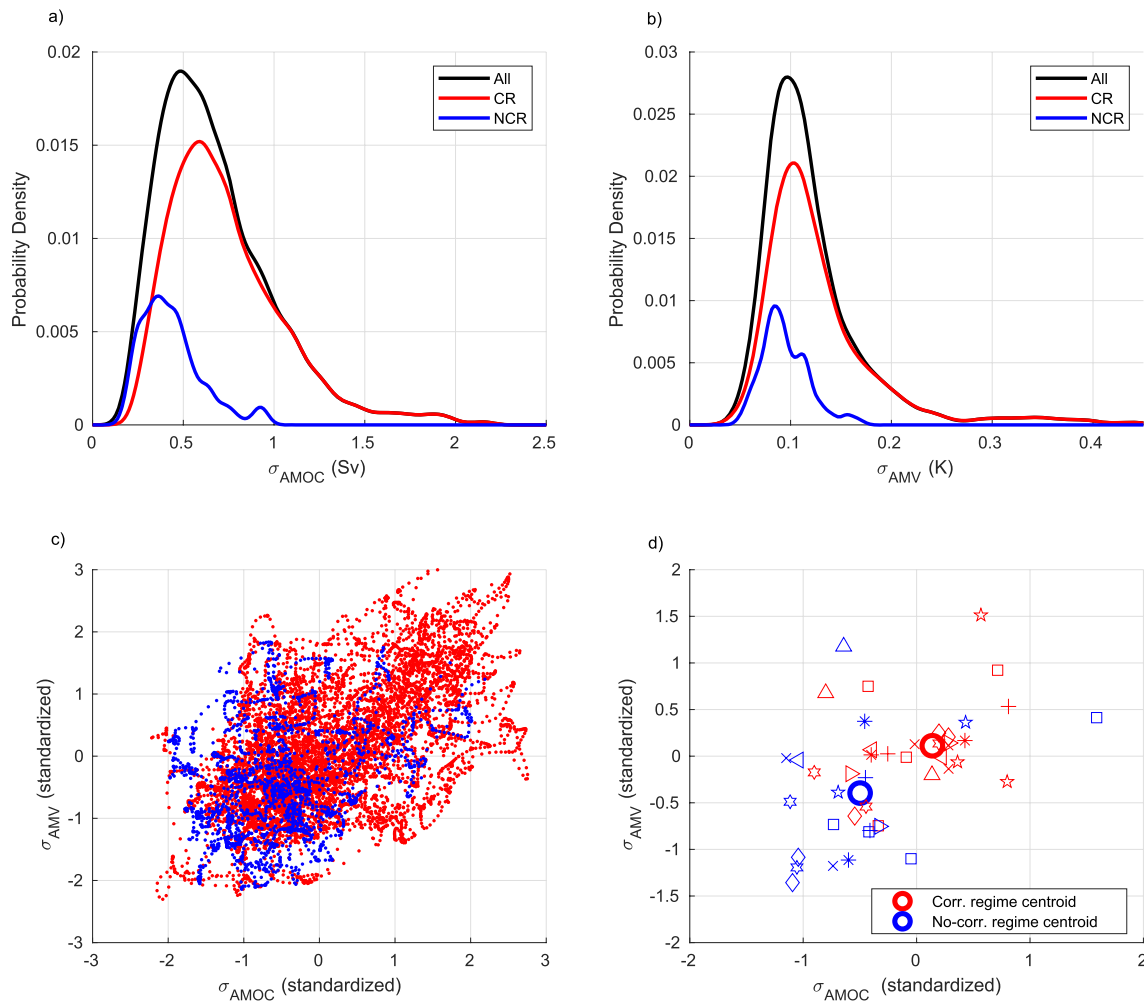


Figure 4. Probability density functions of (a) σ_{AMOC} (Sv) and (b) σ_{AMV} (K) for all models, showing all events (black), *correlated regimes* (CR) events (red) and *non-correlated regimes* (NCR) events (blue). (c) Scatterplot of standardized σ_{AMOC} - σ_{AMV} for all models. CR (NCR) regimes are indicated in red (blue). (d) Same as (c) but now showing centroids corresponding to CR (red) and NCR (blue) events for individual models. Note that each model is identified with a different graphic symbol (see Table S1 in Supporting Information S1) and that for a given model, multiple CR and NCR regimes can be found. Centroids of all CR (NCR) events are shown with a bold, larger-size red (blue) circle.

and on the cumulative effects of all non-AMOC contributions (hereafter schematically referred to as “noise”) we envisage two plausible conceptual models:

1. H1. Stationary AMOC/non-stationary noise: processes other than the AMOC become relatively more important in driving the AMV-like variability, leading to a reduced AMOC-AMV correlation.
2. H2. Non-stationary AMOC/stationary noise: the variability of the AMOC is suppressed, the fraction of AMV explained by AMOC is therefore reduced and the relative weight of a (potentially stationary) noise on the AMV becomes larger, leading to a drop in the AMOC-AMV correlation.

The phenomenological evidence presented in this study suggests that the NCR regimes may be explained by drops in the variability of the AMOC. In this perspective, a less variable oceanic heat transport leads to a suppressed co-variability of the AMV and leaves a larger role for drivers other than the AMOC, ultimately causing a drop of the AMOC-AMV correlation, consistent with H2.

Indeed, Figure 4 shows rather clearly that an uncorrelated regime is very unlikely to be achieved by the system in windows of strong AMOC variability. Using the information provided in Figure 4a, a more quantitative estimate of the likelihood of NCR and CR regimes associated with low and high AMOC variability conditions can be provided, by conventionally setting low- and high- σ_{AMOC} levels equal to the lower and upper terciles of the

full σ_{AMOC} distribution. The probability of finding the system simultaneously in an NCR (CR) regime and a high- σ_{AMOC} state is about 1% (32%). On the other hand, NCR and CR regimes are more equally partitioned in windows of low- σ_{AMOC} variability, with probabilities equal to 15% and 18%, respectively. Thus, correlated and uncorrelated regimes coexist in windows of low-AMOC variability. This indicates that a drop in AMOC variability is not a sufficient condition to have a non-correlated regime. Therefore, the non-stationarity of the noise, while inadequate in explaining the drops of correlation, is still a fundamental ingredient to explain the modeled phenomenology of the AMOC-AMV relationship.

The possible loss of coherence between AMOC and AMV has implications for the predictability of the North Atlantic region. Decadal predictions performed with initialized dynamical models show significant skill in predicting decadal fluctuations in the North Atlantic SSTs, beyond the warming trend. If the claims that this predictability originates from a realistic initialization of the ocean state are robust, then a weakening or disruption of the AMOC-AMV coupling may lead to a consistent loss of predictability over the North Atlantic area.

Finally, these results highlight the potential inadequacy of the currently available instrumental and proxy records for constraining the AMOC-AMV linkage. Model-based results bring the evidence of long-term modulations in the AMOC-AMV variability, which cannot be constrained through historically observed statistics. Assuming that the North Atlantic climate system is currently in a CR regime, transitions toward an NCR regime may be expected in the future. Identifying the precursors of such transitions should be addressed in future studies.

Data Availability Statement

All data from CMIP6 pre-industrial simulations used in our analyses are freely available from the Earth System Grid Federation (<https://esgf-data.dkrz.de/projects/cmip6-dkrz/>). Software used to produce the diagnostics presented in this article is publicly available on the following repository: https://github.com/abellucci/Software-for-GRL_BMRP22.

Acknowledgments

A. B. acknowledges funding from the Italian Ministry of Education, University and Research (MIUR) through the JPI Oceans and JPI Climate “Next Generation Climate Science in Europe for Oceans”—ROADMAP Project (D. M. 593/2016). Open Access Funding provided by Consiglio Nazionale delle Ricerche within the CRUI-CARE Agreement.

References

- Akaike, H. (1974). A new look at the statistical model identification. *IEEE Transactions on Automatic Control*, *19*(6), 716–723. <https://doi.org/10.1109/tac.1974.1100705>
- Ba, J., Keenlyside, N. S., Latif, M., Park, W., Ding, H., Lohmann, K., et al. (2014). A multi-model comparison of Atlantic multidecadal variability. *Climate Dynamics*, *43*(9–10), 2333–2348. <https://doi.org/10.1007/s00382-014-2056-1>
- Bellucci, A., Mariotti, A., & Gualdi, S. (2017). The role of forcings in the twentieth-century North Atlantic multidecadal variability: The 1940–75 North Atlantic cooling case study. *Journal of Climate*, *30*(18), 7317–7337. <https://doi.org/10.1175/jcli-d-16-0301.1>
- Booth, B. B., Dunstone, N. J., Halloran, P. R., Andrews, T., & Bellouin, N. (2012). Aerosols implicated as a prime driver of twentieth-century North Atlantic climate variability. *Nature*, *484*(7393), 228–232. <https://doi.org/10.1038/nature10946>
- Bretherton, C. S., Widmann, M., Dymnikov, V. P., Wallace, J. M., & Bladé, I. (1999). The effective number of spatial degrees of freedom of a time-varying field. *Journal of Climate*, *12*(7), 1990–2009. [https://doi.org/10.1175/1520-0442\(1999\)012<1990:tenosd>2.0.co;2](https://doi.org/10.1175/1520-0442(1999)012<1990:tenosd>2.0.co;2)
- Caesar, L., McCarthy, G. D., Thornalley, D. J. R., Cahill, N., & Rahmstorf, S. (2021). Current Atlantic meridional overturning circulation weakest in last millennium. *Nature Geoscience*, *14*(3), 118–120. <https://doi.org/10.1038/s41561-021-00699-z>
- Clement, A., Bellomo, K., Murphy, L. N., Cane, M. A., Mauritzen, T., Rädel, G., & Stevens, B. (2015). The Atlantic Multidecadal Oscillation without a role for ocean circulation. *Science*, *350*(6258), 320–324. <https://doi.org/10.1126/science.aab3980>
- Delworth, T. L., & Mann, M. E. (2000). Observed and simulated multidecadal variability in the Northern Hemisphere. *Climate Dynamics*, *16*(9), 661–676. <https://doi.org/10.1007/s003820000075>
- Eyring, V., Bony, S., Meehl, G., Senior, C. A., Stevens, B., Stouffer, R. J., & Taylor, K. E. (2016). Overview of the Coupled Model Intercomparison Project Phase 6 (CMIP6) experimental design and organization. *Geoscientific Model Development*, *9*(5), 1937–1958. <https://doi.org/10.5194/gmd-9-1937-2016>
- Gulev, S., Latif, M., Keenlyside, N., Park, W., & Koltermann, K. P. (2013). North Atlantic Ocean control on surface heat flux on multidecadal timescales. *Nature*, *499*(7459), 464–467. <https://doi.org/10.1038/nature12268>
- Haynes, K., Eckley, I. A., & Fearnhead, P. (2014). Efficient penalty search for multiple change-point problems. arXiv: 1412.3617.
- Jiang, W., Gastineau, G., & Codron, F. (2021). Multicentennial variability driven by salinity exchanges between the Atlantic and the Arctic Ocean in a coupled climate model. *Journal of Advances in Modeling Earth Systems*, *13*(3), e2020MS002366. <https://doi.org/10.1029/2020ms002366>
- Killick, R., Fearnhead, P., & Eckley, I. A. (2012). Optimal detection of change-points with a linear computational cost. *Journal of the American Statistical Association*, *107*(500), 1590–1598. <https://doi.org/10.1080/01621459.2012.737745>
- Knight, J. R., Allan, R. J., Folland, C. K., Vellinga, M., & Mann, M. E. (2005). A signature of persistent natural thermohaline circulation cycles in observed climate. *Geophysical Research Letters*, *32*(20), L2070. <https://doi.org/10.1029/2005gl024233>
- Mann, M. E., Steinman, B. A., Brouillette, D. J., & Miller, S. K. (2021). Multidecadal climate oscillations during the past millennium driven by volcanic forcing. *Science*, *371*(6533), 1014–1019. <https://doi.org/10.1126/science.abc5810>
- Mavilia, I., Bellucci, A., Athanasiadis, P. J., Gualdi, S., Msadek, R., & Ruprich-Robert, Y. (2018). On the spectral characteristics of the Atlantic multidecadal variability in an ensemble of multi-century simulations. *Climate Dynamics*, *51*(9–10), 3507–3520. <https://doi.org/10.1007/s00382-018-4093-7>
- Otterå, O. H., Bentsen, M., Drange, H., & Suo, L. (2010). External forcing as a metronome for Atlantic multidecadal variability. *Nature Geoscience*, *3*(10), 688–694. <https://doi.org/10.1038/ngeo955>

- Robson, J., Sutton, R., & Smith, D. (2014). Decadal predictions of the cooling and freshening of the North Atlantic in the 1960s and the role of ocean circulation. *Climate Dynamics*, 42(9–10), 2353–2365. <https://doi.org/10.1007/s00382-014-2115-7>
- Scott, D. W. (1992). *Multivariate density estimation: Theory, practice, and visualization*. John Wiley & Sons.
- Swingedouw, D., Ortega, P., Mignot, J., Guilyardi, E., Masson-Delmotte, V., Butler, P. G., et al. (2015). Bidecadal North Atlantic ocean circulation variability controlled by timing of volcanic eruptions. *Nature Communications*, 6(1), 6545. <https://doi.org/10.1038/ncomms7545>
- Tandon, N. F., & Kushner, P. J. (2015). Does external forcing interfere with the AMOC's influence on North Atlantic sea surface temperature? *Journal of Climate*, 28(16), 6309–6323. <https://doi.org/10.1175/jcli-d-14-00664.1>
- Torrence, C., & Compo, G. P. (1998). A practical guide to wavelet analysis. *Bulletin of the American Meteorological Society*, 79(1), 61–78. [https://doi.org/10.1175/1520-0477\(1998\)079<0061:apgtwa>2.0.co;2](https://doi.org/10.1175/1520-0477(1998)079<0061:apgtwa>2.0.co;2)
- Wittenberg, A. T. (2009). Are historical records sufficient to constrain ENSO simulations? *Geophysical Research Letters*, 36(12), L12702. <https://doi.org/10.1029/2009gl0138710>
- Yeager, S. G., & Robson, J. (2017). Recent progress in understanding and predicting Atlantic decadal climate variability. *Current Climate Change Reports*, 3(2), 112–127. <https://doi.org/10.1007/s40641-017-0064-z>
- Zhang, R., Sutton, R., Danabasoglu, G., Kwon, Y.-O., Marsh, R., Yeager, S. G., et al. (2019). A review of the role of the Atlantic meridional overturning circulation in Atlantic multidecadal variability and associated climate impacts. *Reviews of Geophysics*, 57(2), 316–375. <https://doi.org/10.1029/2019rg000644>

References From the Supporting Information

- Boucher, O., Servonnat, J., Albright, A., Aumont, O., Balkanski, Y., Bastrikov, V., et al. (2020). Presentation and evaluation of the IPSL-CM6A-LR climate model. *Journal of Advances in Modeling Earth Systems*, 12(7), e2019MS002010. <https://doi.org/10.1029/2019MS002010>
- Danabasoglu, G., Lamarque, J.-F., Bacmeister, J., Bailey, D. A., DuVivier, A. K., Edwards, J., et al. (2020). The community Earth system model version 2 (CESM2). *Journal of Advances in Modeling Earth Systems*, 12, e2019MS001916. <https://doi.org/10.1029/2019ms001916>
- Döscher, R., Acosta, M., Alessandri, A., Anthoni, P., Arneth, A., Arsouze, T., et al. (2022). The EC-Earth3 Earth system model for the climate model Intercomparison Project 6. *Geoscientific Model Development*, 15, 2973–3020.
- Mauritsen, T., Bader, J., Becker, T., Behrens, J., Bittner, M., Brokopf, R., et al. (2019). Developments in the MPI-M Earth System Model version 1.2 (MPI-ESM1.2) and its response to increasing CO₂. *Journal of Advances in Modeling Earth Systems*, 11(4), 998–1038. <https://doi.org/10.1029/2018ms001400>
- Park, S., Shin, J., Kim, S., Oh, E., & Kim, Y. (2019). Global climate simulated by the Seoul National University atmosphere model version 0 with a Unified convection scheme (SAM0-UNICON). *Journal of Climate*, 32(10), 2917–2949. <https://doi.org/10.1175/jcli-d-18-0796.1>
- Swart, N. C., Cole, J. N. S., Kharin, V. V., Lazare, M., Scinocca, J. F., Gillett, N. P., et al. (2019). The Canadian Earth system model version 5 (CanESM5.0.3). *Geoscientific Model Development*, 12(11), 4823–4873. <https://doi.org/10.5194/gmd-12-4823-2019>
- Volodin, E. M., Mortikov, E. V., Kostykin, S. V., Galin, V. Y., Lykossov, V. N., Gritsun, A. S., et al. (2017). Simulation of the present-day climate with the climate model INMCM5. *Climate Dynamics*, 49(11–12), 3715–3734. <https://doi.org/10.1007/s00382-017-3539-7>
- Yukimoto, S., Kawai, H., Koshiro, T., Oshima, N., Yoshida, K., Urakawa, S., et al. (2019). The Meteorological Research institute Earth System Model version 2.0, MRI-ESM2.0: Description and basic evaluation of the physical component. *Journal of the Meteorological Society of Japan. Ser. II*, 97(5), 931–965. <https://doi.org/10.2151/jmsj.2019-051>